Environ Fluid Mech (2009) 9:125–142
DOI 10.1007/s10652-008-9078-3

ORIGINAL ARTICLE

Turbulent air–water flows in hydraulic structures: dynamic similarity and scale effects

H. Chanson

Received: 12 December 2007 / Accepted: 30 May 2008 / Published online: 25 June 2008
© Springer Science+Business Media B.V. 2008

Abstract In hydraulic structures, free-surface aeration is commonly observed: i.e., the white waters. The air bubble entrainment may be localised (hydraulic jumps, plunging jets) or continuous along an interface (water jets, chutes). Despite recent advances, there are some basic concerns about the extrapolation of laboratory results to large size prototype structures. Herein the basic air bubble entrainment processes are reviewed and the relevant dynamic similarities are discussed. Traditionally, physical studies are conducted using a Froude similitude which implies drastically smaller laboratory Reynolds numbers than in the corresponding prototype flows. Basic dimensional analyses are developed for both singular and interfacial aeration processes. The results are discussed in the light of systematic investigations and they show that the notion of scale effects is closely linked with the selection of relevant characteristic air–water flow properties. Recent studies of local air–water flow properties highlight that turbulence levels, entrained bubble sizes and interfacial areas are improperly scaled based upon a Froude similitude even in large-size models operating with the so defined Reynolds numbers $\rho_w \times q_w/\mu_w$ up to 5 E+5. In laboratory models, the dimensionless turbulence levels, air–water interfacial areas and mass transfer rates are drastically underestimated.

Keywords Air–water flows · Air bubble entrainment · Turbulence · Hydraulic engineering · Dynamic similarity · Scale effects · Froude similitude · Plunging jets · Hydraulic jumps · Spillway chutes · Stepped spillways · High-velocity water jets

1 Introduction

Air bubble entrainment is defined as the entrapment of air bubbles and pockets that are advected within the turbulent flow. The entrainment of air packets can be localised or continuous along the air–water interface. Examples of localised aeration include air entrainment

H. Chanson (✉)
Division of Civil Engineering, The University of Queensland, Brisbane, QLD 4072, Australia
e-mail: h.chanson@uq.edu.au
URL: http://www.uq.edu.au/∼e2hchans/

by plunging jet and at hydraulic jump. Bubbles are entrained locally at the intersection of the impinging jet with the surrounding waters (Fig. 1b). The intersecting perimeter is a singularity in terms of both air entrainment and momentum exchange, and the air is entrapped at the discontinuity between the impinging jet flow and the receiving pool of water. Interfacial aeration is defined as the air entrainment process along an air–water interface, usually parallel to the flow direction (Fig. 1a, c). Figure 1a illustrates interfacial aeration along the free-surface of high-velocity water jets discharging into the atmosphere. Figure 1b presents an example of plunging jet aeration at the toe of a drop spillway, while Fig. 1c shows interfacial aeration down a stepped spillway.

Air–water flows have been studied relatively recently. The first successful experimental investigations were conducted during the mid-20th century [31,49]. Important contributions included Rajaratnam [45] and Resch and Leutheusser [47] on hydraulic jumps, and Heraud [37] and Hoyt and Taylor [39] on high-velocity water jets. A seminal study was the series of experiments performed on the Aviemore dam spillway in New Zealand [7,8,40]. Both laboratory and prototype investigations showed the complexity of the free-surface aeration process and some recent studies highlighted the strong interactions between entrained bubbles and turbulence (e.g., [6,16,21]). These significant findings are not complete despite several book publications [13,41,46,51]. There are still some fundamental reservations about the extrapolation of laboratory results to a large size prototype as shown in Fig. 1a.

The aim of the present study is to review the basic air bubble entrainment processes in hydraulic structures, and to discuss the relevant dynamic similarities and associated scale effects. After a review of some basic mechanisms, both singular and interfacial aeration processes are considered. The outcomes are discussed in the light of recent experimental works.

2 Basic mechanisms of air bubble entrainment

2.1 Onset of air bubble entrainment

The onset of air entrainment is defined as a threshold situation above which air entrainment takes place. While there is some distinction between the first bubble entrapment and the start of continuous air bubble entrainment, the corresponding flow conditions fall usually within a very narrow range called broadly the inception conditions. Early studies expressed the inception conditions as functions of a time-averaged velocity. For example, air entrainment in turbulent water flows occurs when the flow velocity exceeds roughly 0.5–2 m/s. The approach does not account for the complexity of the flow nor the turbulence properties. Although present knowledge remains empirical and often superficial, recent studies linked the onset of air entrainment with a characteristic level of normal Reynolds stresses next to the free-surface. For example, Ervine and Falvey [33] and Chanson [11] in water jets and steep chute flows, Cummings and Chanson [30] for plunging jets, Brocchini and Peregrine [6]. A summary of experimental results for vertical plunging water jets is presented in Fig 2. Figure 2 shows the dimensionless onset velocity $\mu_w V/\sigma$ as a function of the dimensionless normal turbulent stress v'^2/V^2 where V is the jet velocity at impingement, v' is the root mean square of the instantaneous jet velocity, μ_w is the water dynamic viscosity and σ is the surface tension between air and water. All the data collapse into a well-defined trend shown as a dashed line in Fig. 2.

It is argued that the inception of air entrainment is linked with a characteristic level of tangential Reynolds stresses next to the free-surface. Experimental evidences showed that

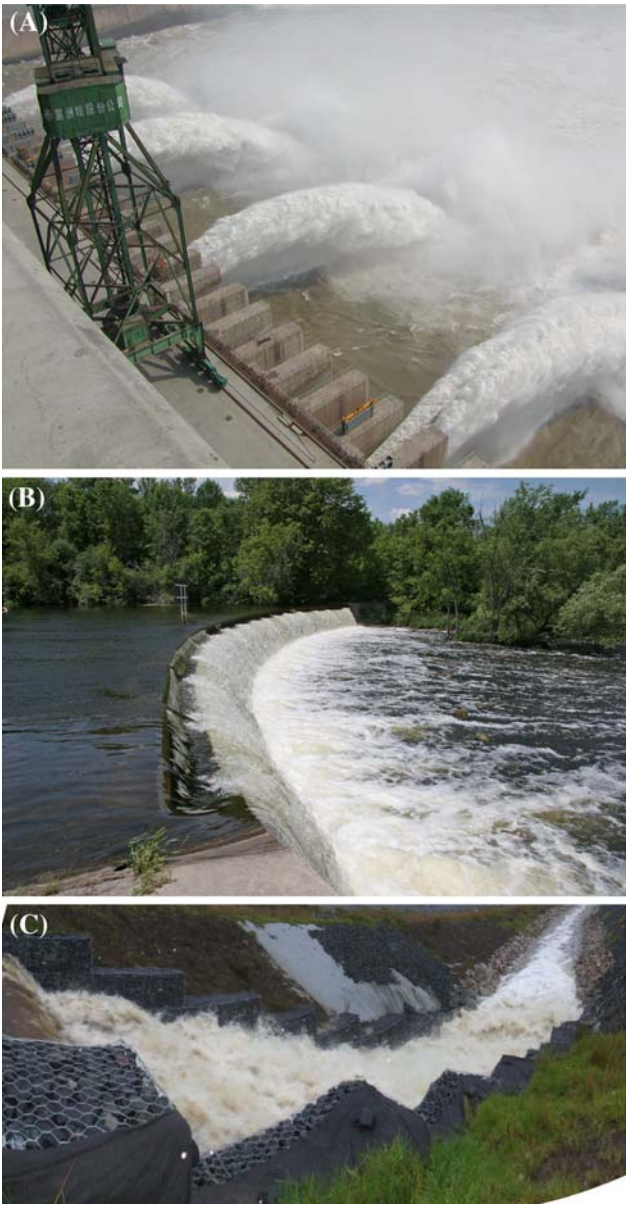

Fig. 1 Air entrainment in hydraulic structures (**a**) Free-surface aeration at the bottom outlet of the Three Gorges Dam, China on 20 October 2004—$Q_w = 1700\,m^3/s$ per jet, $V_1 = 35\,m/s$, $d_1 = 7\,m$, $W = 9\,m$ (**b**) Plunging jet aeration at the toe of Nicholsons Dam, Canada in June 2006 (Courtesy of Ken WATSON) (**c**) Interfacial aeration down a stepped chute on 8 June 2007 (Courtesy of Tony MARSZALEK)—Stepped chute: $\theta = 18.4°$, $h = 1\,m$, $l = 3\,m$, $W = 8\,m$, flow from top left to bottom right

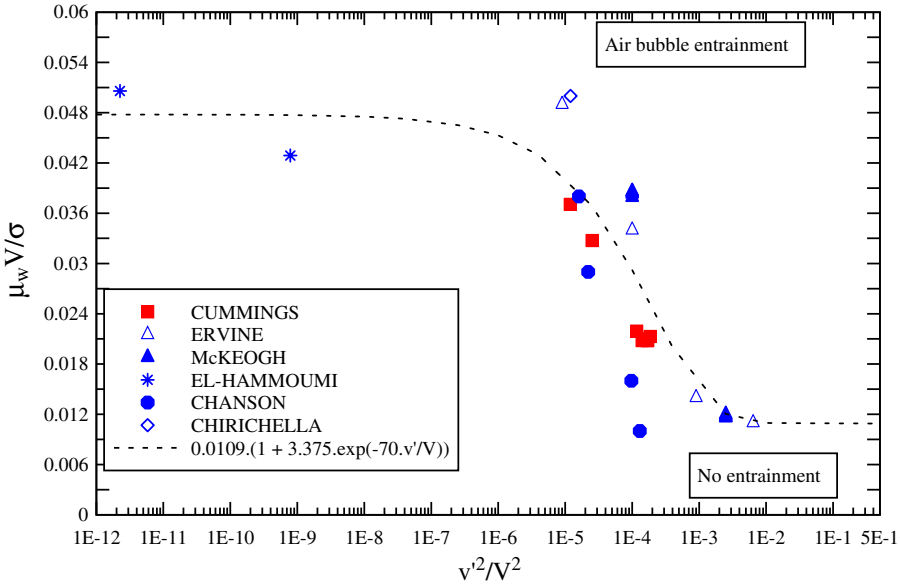

Legend	Reference	Configuration
CUMMINGS	CUMMINGS and CHANSON (1999)	Two-dimensional supported jets (d = 12 mm)
ERVINE	ERVINE et al. (1980)	Circular jets (∅ =6 to 25 mm)
McKEOGH	McKEOGH (1978)	Circular jets (∅ =2.8 to 14 mm)
EL-HAMMOUMI	EL-HAMMOUMI (1994)	Circular jets (∅ =9 to 16 mm)
CHANSON	CHANSON and MANASSEH (2003)	Circular jets (∅ =24 mm)
CHIRICHELLA	CHIRICHELLA et al. (2002)	Circular jets (∅ =6 mm)

Fig. 2 Onset of air bubble entrainment in vertical plunging jets in freshwater

the free-surface of turbulent flows exhibits some surface "undulations" with a fine-grained turbulent structure and larger underlying eddies [1,39] (Fig. 3). Air entrainment occurs when the turbulent shear stress next to the interface is large enough to overcome both surface tension and buoyancy effects if any. Since the turbulent energy is high in small eddy lengths close to the free surface, air bubble entrainment may result from the action of high intensity turbulent shear close to the air–water interface. Free-surface breakup and bubble entrapment occurs when the turbulent shear stress is greater than the capillary force per unit area resisting the surface breakup. For an elongated spheroid, it yields:

$$\left|\rho_w v_i v_j\right| > \sigma \frac{\pi \times (r_1 + r_2)}{A} \qquad \text{onset condition} \tag{1}$$

where ρ_w is the water density, v is the instantaneous turbulent velocity fluctuation, (i, j) is the directional tensor (i, j = x, y, z), $\pi \times (r_1 + r_2)$ is the perimeter along which surface tension acts, r_1 and r_2 are the two principal radii of curvature of the free surface deformation, and A is surface deformation area. Equation 1 gives a criterion for the onset of free-surface aeration in terms of the magnitude of the instantaneous tangential Reynolds stress, the air/water physical properties and the free-surface deformation properties. Air bubbles cannot be entrained across the free-surface until there is sufficient tangential shear relative to the surface tension force per unit area.

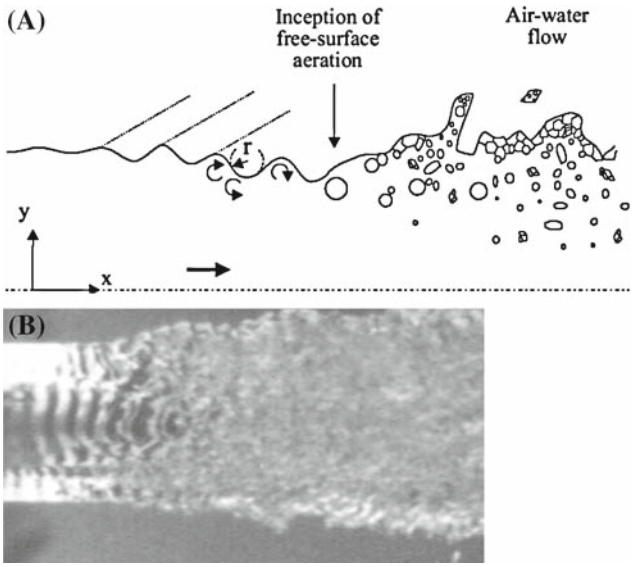

Fig. 3 Onset of air bubble entrainment in free-surface flows (**a**) Definition sketch (**b**) Free-surface instability upstream of the inception point of air entrainment in a high-velocity jet (Courtesy of Professor J.W. HOYT)—flow from left to right, circular jet (D = 3.5 mm), V = 19.5 m/s

For a three-dimensional flow with quasi-isotropic turbulence, the smallest interfacial area per unit volume of air is the sphere (radius r). Equation 1 gives a condition for the onset of spherical bubble entrainment:

$$\left|\rho_w v_i v_j\right| > \frac{\sigma}{2\pi r} \tag{2}$$

Equation 2 implies that the onset of air bubble entrainment takes place predominantly in the form of relatively large bubbles. But the largest bubbles are detrained by buoyancy and this yields some preferential size of entrained bubbles observed to be about 1–100 mm in prototype turbulent flows (e.g., [7,11,13]).

2.2 Bubble breakup

Once entrained, the air bubbles are advected in a turbulent shear flow. In regions of strong momentum mixing, the entrained air is broken into smaller bubbles. In an equilibrium situation, a maximum bubble size may be estimated by the balance between the surface tension force and the inertial force caused by the velocity changes over distances of the order of the bubble size. Some simple dimensional analysis yielded a criterion for bubble breakup [38]. The result is however limited because equilibrium situations are rare, and it is simply not applicable in many turbulent shear flows.

In turbulent air–water flows, experimental observations implied that the air bubble sizes are larger than the Kolmogorov microscale and smaller than the turbulent macroscale [13]. These suggested that the length scale of the vortices responsible for breaking up the bubbles is close to the bubble size. Larger eddies advect the bubbles while eddies with length-scales substantially smaller than the bubble size do not have the required energy to break up the bubbles. In a shear flow, the bubble break-up occurs when the tangential shear stress is greater than the capillary force per unit area:

$$\left|\rho_w v_i v_j\right| > \frac{\sigma}{\pi d_{ab}} \tag{3}$$

where d_{ab} is the bubble diameter. Equation 3 applies to a spherical bubble and the left handside term is the magnitude of the instantaneous tangential Reynolds stress. The approach may be extended to non-spherical bubbles. For an elongated spheroid, bubble breakup takes place for:

$$\left|\rho_w v_i v_j\right| > \sigma \frac{\pi \ (r_1 + r_2)}{2 \times \pi \times r_1 \left(r_1 + r_2 \times \dfrac{\text{Arc}\sin\left(\sqrt{1 - \dfrac{r_1{}^2}{r_2{}^2}}\right)}{\sqrt{1 - \dfrac{r_1{}^2}{r_2{}^2}}} \right)} \tag{4}$$

where r_1 and r_2 are the equatorial and polar radii of the ellipsoid respectively with $r_2 > r_1$. Equation 4 highlights that some turbulence anisotropy (e.g., $v_x, \gg v_y, v_z$) must induce some preferential bubble shapes.

2.3 Buoyancy effects on submerged bubbles

When an air bubble is submerged in a liquid, the buoyancy force is the vertical resultant of the pressure forces acting on the bubble. Its expression may be derived from the integration of the pressure field around the bubble and it is directly proportional to minus the pressure gradient $\partial P/\partial z$ where P is the pressure and z is the vertical axis positive upwards. The effects of buoyancy on a submerged air bubble may be expressed in terms of the bubble rise velocity u_r which may be estimated in a non-hydrostatic pressure gradient to a first approximation as:

$$u_r = \pm (u_r)_{Hyd} \sqrt{\frac{\left|\frac{\partial P}{\partial Z}\right|}{\rho_w \ g}} \tag{5}$$

where $(u_r)_{Hyd}$ is the bubble rise velocity in a hydrostatic pressure gradient and g is the gravity acceleration. The sign of the rise velocity u_r depends on the sign of $\partial P/\partial z$.

Considering a self-aerated open channel flow, the fluid density at a distance y from the invert is $\rho_w(1 - C)$ where C is the local void fraction, and the expression of the bubble rise velocity becomes:

$$\frac{u_r}{(u_r)_{Hyd}} = \sqrt{1 - C} \tag{6}$$

Equation 6 expresses the rise velocity of a bubble in an air–water mixture of void fraction C as a function of the rise velocity in hydrostatic pressure gradient [12,13]. It shows that the buoyant force is smaller in aerated waters than in clear-water. This fact is well known to river surfers who use large surf boards for greater buoyancy volume.

3 Dynamic similarity in hydraulic jumps and plunging jet flows

3.1 Dimensional analysis

In hydraulic jumps and plunging jets, the source of air bubble entrainment is localised at a flow discontinuity: i.e., the intersection of the impinging water jet with the receiving body of

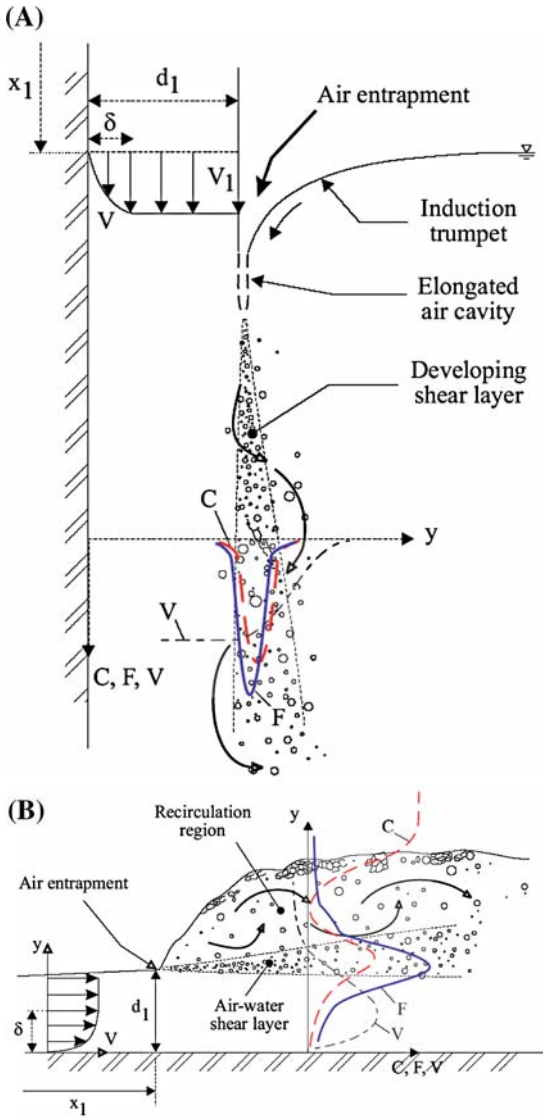

Fig. 4 Definition sketches of singular air bubble entrainment (**a**) Air entrainment at a vertical two-dimensional plunging jet (**b**) Air entrainment at a hydraulic jump

water (Fig. 4). Figure 4a presents a sketch of a vertical plunging jet flow, while Fig. 4b shows a horizontal plunging jet flow that is a hydraulic jump. The air bubbles are entrained locally at the flow singularity and the impingement perimeter is a source of air bubbles as well as a source of vorticity. But vorticity and air bubbles are diffused in a different manner and at a different rate yielding some double diffusion process.

Theoretical and numerical studies of air–water turbulent flows are complicated by the large number of relevant equations: i.e., three basic equations (continuity, momentum, energy) for each phase, plus a mass transfer equation. Therefore most studies rely upon some physical experiments with sophisticated instrumentations [5,10,14,29]. Laboratory model studies are performed under controlled flow conditions with geometrically similar models.

In a dimensional analysis, the relevant parameters include the fluid properties and physical constants, the channel geometry and inflow conditions, the air–water flow properties including the entrained air bubble characteristics and turbulence characteristics. Considering a horizontal hydraulic jump, or a vertical two-dimensional supported plunging jet, a simplified dimensional analysis shows that the parameters affecting the air–water flow properties at a position (x, y, z) are: (a) the fluid properties including the air and water densities ρ_{air} and ρ_w, the air and water dynamic viscosities μ_{air} and μ_w, the surface tension σ, and the gravity acceleration g, (b) the channel properties including the width W, and, (c) the impingement flow properties such as the inflow depth d_1, the inflow velocity V_1, a characteristic turbulent velocity u'_1, and the boundary layer thickness δ (Fig. 4) The dimensionless air–water flow properties may be expressed as:

$$C, \frac{Fd_1}{V_1}, \frac{V}{\sqrt{gd_1}}, \frac{u'}{V_1}, \frac{d_{ab}}{d_1} \ldots = F_1\left(\frac{x}{d_1}, \frac{y}{d_1}, \frac{z}{d_1}, \frac{V_1}{\sqrt{gd_1}}, \frac{u'_1}{V_1}, \rho_w \frac{V_1 d_1}{\mu_w}, \rho_w \frac{{V_1}^2 d_1}{\sigma}, \frac{x_1}{d_1}, \frac{\delta}{d_1}, \frac{W}{d_1}, \text{Salinity}, \ldots\right) \tag{7}$$

where C is the void fraction, F is the bubble count rate, V is the velocity, u' is a characteristic turbulent velocity, d_{ab} is a bubble size, x is the coordinate in the flow direction measured from the nozzle, y is the normal coordinate, z is the transverse coordinate measured from the channel centreline, and x_1 is the distance from the upstream gate or nozzle. In addition, biochemical properties of the water solution may be considered. If the local void fraction C is known, the density and viscosity of the air–water mixture may be expressed in terms of the water properties and void fraction only; hence the parameters ρ_{air} and μ_{air} may be ignored.

In Eq. 7, the dimensionless air–water flow properties (left handside terms) at a dimensionless position (x/d_1, y/d_1, z/d_1) are expressed as functions of the dimensionless inflow properties and channel geometry. In the right handside of Eq. 7, the fourth, sixth and seventh terms are the inflow Froude, Reynolds and Weber numbers respectively. Any combination of these numbers is also dimensionless and may be used to replace one of the combinations. In particular one parameter can be replaced by the Morton number $Mo = g{\mu_w}^4/(\rho_w \sigma^3)$ which becomes an invariant if the same fluids (air and water) are used in model and prototype. It yields:

$$C, \frac{Fd_1}{V_1}, \frac{V}{\sqrt{gd_1}}, \frac{u'}{V_1}, \frac{d_{ab}}{d_1} \ldots = F_2\left(\frac{x}{d_1}, \frac{y}{d_1}, \frac{z}{d_1}, \frac{V_1}{\sqrt{gd_1}}, \frac{u'_1}{V_1}, \rho_w \frac{V_1 d_1}{\mu_w}, \frac{g{\mu_w}^4}{\rho_w \sigma^3}, \frac{x_1}{d_1}, \frac{\delta}{d_1}, \frac{W}{d_1}, \text{Salinity}, \ldots\right) \tag{8}$$

3.2 Dynamic similarity and scaling laws

In a geometrically similar model, a true dynamic similarity is achieved if and only if each dimensionless parameter has the same value in both model and prototype. Scale effects may exist when one or more dimensionless terms have different values between model and prototype. Despite the simplistic assumption, Eqs. 7 and 8 demonstrate that dynamic similarity of air bubble entrainment at plunging jets and in hydraulic jumps is impossible with geometrically similar models because of the too many relevant dimensionless parameters.

In the study of free-surface flows including hydraulic jumps and plunging jets, a Froude similitude is commonly used because the gravity effects are dominant (e.g., [15,36]). That is, the model and prototype Froude numbers must be equal. However the entrapment of

air bubbles and the mechanisms of air bubble breakup and coalescence are dominated by surface tension effects, while turbulent processes in the shear region are dominated by viscous forces [13,51]. Dynamic similarity of air bubble entrainment in hydraulic jumps becomes impossible because of too many relevant parameters (e.g., Froude, Reynolds and Morton numbers) in Eq. 8. For example, with the same fluids (air and water) in model and prototype, the air entrainment process is adversely affected by significant scale effects in small size models [41]. Figure 5 illustrates three hydraulic jumps with identical inflow Froude numbers but different inflow Reynolds numbers. In the smallest channel (Fig. 5a), drastically lesser bubble entrainment was observed [44].

A few studies investigated systematically the air–water flow properties in hydraulic jumps and plunging jets with geometrically similar models under controlled flow conditions (Table 1). These were based upon a Froude similitude with undistorted models. Despite the limited number of systematic studies, the results of the investigations listed in Table 1 highlighted the limitations of dynamic similarity and physical modelling of air–water flows. In hydraulic jumps, experiments with $\rho_w V_1 d_1/\mu_w$ up to 1 E+5 could not be extrapolated to larger prototypes without significant scale effects. At vertical circular plunging jets, drastic scale effects were observed for $\rho_w {V_1}^2 d_1/\sigma < 1\,\text{E+3}$.

The same studies showed further that the selection of the criteria to assess scale affects is critical: the void fraction distributions, the bubble count rate distributions, the distributions of bubble chords. Simply the experimental results demonstrated that scale effects may be significant [26,19]. At the limit no scale effect is observed at full scale only ($L_r = 1$) using the same fluids in model and prototype. The geometric scaling ratio L_r is defined herein as the ratio of prototype to model dimensions.

4 Dynamic similarity in self-aerated chute flows and water jets

In self-aerated chute flows and at turbulent water jets discharging into the atmosphere, the entrainment of air bubbles is continuous along the air–water free-surface: i.e., some interfacial aeration mechanism. The air bubble entrainment process takes place along an air–water interface usually parallel to the flow direction and the entrained air bubbles are advected in the shear flow (Fig. 6). Figure 6a shows a high-velocity jets discharging into the atmosphere, and Fig. 6b presents a self-aerated skimming flow down a stepped chute.

Considering a supercritical open channel flow down a prismatic rectangular smooth chute, a complete dimensional analysis yields:

$$C, \frac{Fd_c}{V_c}, \frac{V}{\sqrt{gd_c}}, \frac{u'}{V_c}, \frac{d_{ab}}{d_c} \ldots = F_3\left(\frac{x}{d_c}, \frac{y}{d_c}, \frac{z}{d_c}, \rho_w \frac{\sqrt{gd_c{}^3}}{\mu_w}, \frac{g\mu_w{}^4}{\rho_w \sigma^3}, \frac{W}{d_c}, \theta, \frac{k_s}{d_c}, \ldots\right) \quad (9)$$

where d_c is the critical flow depth ($d_c = \sqrt[3]{{q_w}^2/g}$), q_w is the water discharge per unit width, W is the channel width, θ is the invert slope, and k_s is the equivalent roughness height. In Eq. 9 right handside, the fourth and fifth dimensionless terms are the Reynolds and Morton numbers respectively, and the last three terms characterise the chute geometry and the skin friction effects on the invert and sidewalls. The selection of the critical depth d_c as the characteristic length scale assumes implicitly a Froude similitude since the ratio of the equivalent clear-water depth d to the critical flow depth is:

$$\frac{d}{d_c} = \sqrt[3]{\frac{gd^3}{{q_w}^2}} = Fr^{-2/3} \quad (10)$$

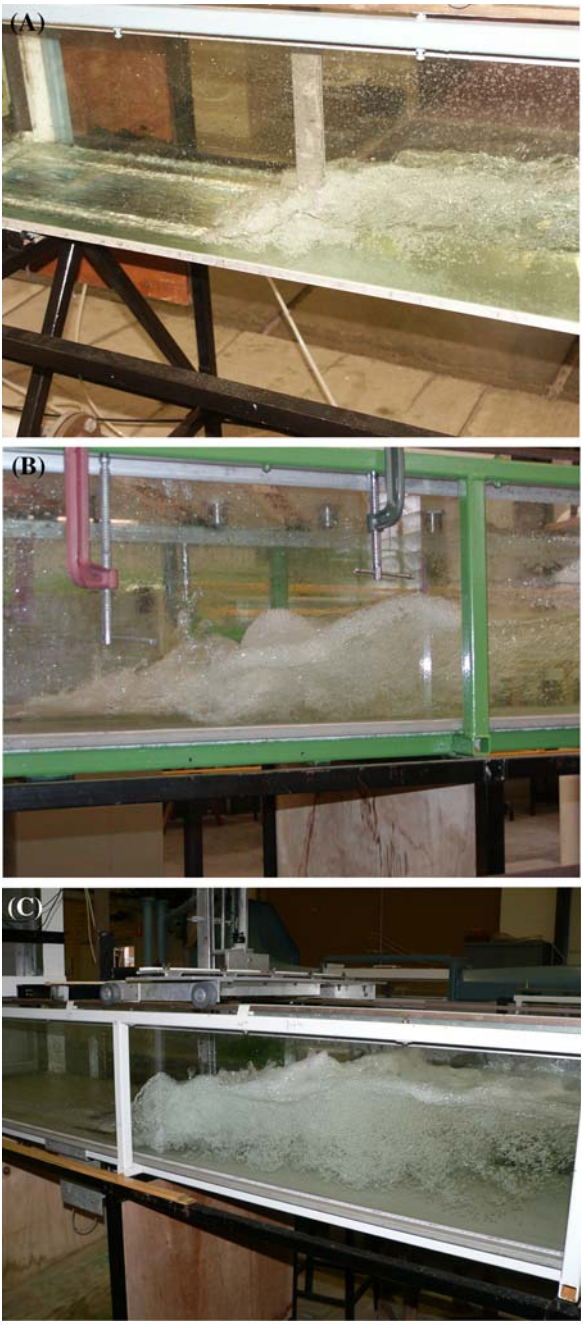

Fig. 5 Photographs of air bubble entrainment in hydraulic jumps for $V_1/\sqrt{gd_1} = 5$ (flow from left to right) (**a**) $V_1/\sqrt{gd_1} = 5.1$, $\rho_w V_1 d_1/\mu_w = 2.4\,E{+}4$, $x_1 = 0.5\,m$, $W = 0.25\,m$ (shutter speed: 1/60 s) (**b**) $V_1/\sqrt{gd_1} = 5.1$, $\rho_w V_1 d_1/\mu_w = 3.8\,E{+}4$, $x_1 = 0.5\,m$, $W = 0.5\,m$ (shutter speed: 1/40 s) (**c**) $V_1/\sqrt{gd_1} = 5.3$, $\rho_w V_1 d_1/\mu_w = 7.1\,E{+}4$, $x_1 = 1\,m$, $W = 0.5\,m$ (shutter speed: 1/80 s)

Table 1 Systematic studies of dynamic similarity and scale effects of air-water flow properties in plunging jets and hydraulic jumps

Study (1)	Similitude (2)	Experimental flow conditions (3)	Instrumentation (4)	Experimental data (5)
Plunging jet flows				
[26]	Froude	Vertical circular jets: $d_1 = 0.025, 0.0125, 0.0068$ m $7 < V_1/\sqrt{gd_1} < 10$ $3\,E{+}3 < \rho_w V_1 d_1/\mu_w < 2\,E{+}5$ Freshwater $L_r = 1, 2, 3.66$	Single-tip conductivity probe (Ø = 0.35 & 0.1 mm)	Void fraction & bubble count rate distributions, Bubble sizes
[27]	Froude	Vertical circular jets: $d_1 = 0.0125$ m $7 < V_1/\sqrt{gd_1} < 10$ $2\,E{+}4 < \rho_w V_1 d_1/\mu_w < 4\,E{+}4$ Freshwater, artificial saltwater and natural seawater $L_r = 1$	Single-tip conductivity probe (Ø = 0.1 mm)	Void fraction & bubble count rate distributions, Bubble sizes
Hydraulic jumps				
[19]	Froude	Horizontal hydraulic jumps: $d_1 = 0.012$ & 0.024 m $W = 0.25$ & 0.5 m $V_1/\sqrt{gd_1} = 5, 6.5, 8.5$ $2.4\,E{+}4 < \rho_w V_1 d_1/\mu_w < 9.8\,E{+}4$ $L_r = 1, 2$	Single-tip conductivity probe (Ø = 0.35 mm)	Void fraction & bubble count rate distributions, Bubble chord times
[44]	Froude	Horizontal hydraulic jumps: $d_1 = 0.012, 0.018$ & 0.024 m $W = 0.25$ & 0.5 m $V_1/\sqrt{gd_1} = 5, 8.5$ $2.4\,E{+}4 < \rho_w V_1 d_1/\mu_w < 9.8\,E{+}4$ $L_r = 1, 1.33, 2$	Single-tip conductivity probe (Ø = 0.35 mm) & Double-tip conductivity probe (Ø = 0.25 mm)	Void fraction & bubble count rate distributions, Bubble chord times

Notes: L_r, geometric scaling ratio; W, channel width

where the equivalent clear-water depth is derived from the void fraction distribution:

$$d = \int_{y=0}^{y=Y_{90}} (1 - C)\, dy \tag{11}$$

with y the distance normal to the invert and Y_{90} the characteristic depth where $C = 0.90$.

At uniform equilibrium (i.e., normal flow conditions), further simplifications may be derived by considering the depth-averaged air–water flow properties which become invariant of the longitudinal location. For a smooth chute flow at uniform equilibrium, Eq. 9 becomes:

$$F_4\left(\frac{U_w}{\sqrt{gd}}, \rho_w \frac{U_w d}{\mu_w}, \frac{g{\mu_w}^4}{\rho_w \sigma^3}, C_{mean}, \frac{W}{d}, \theta, \frac{k_s}{d}, \ldots\right) = 0 \tag{12}$$

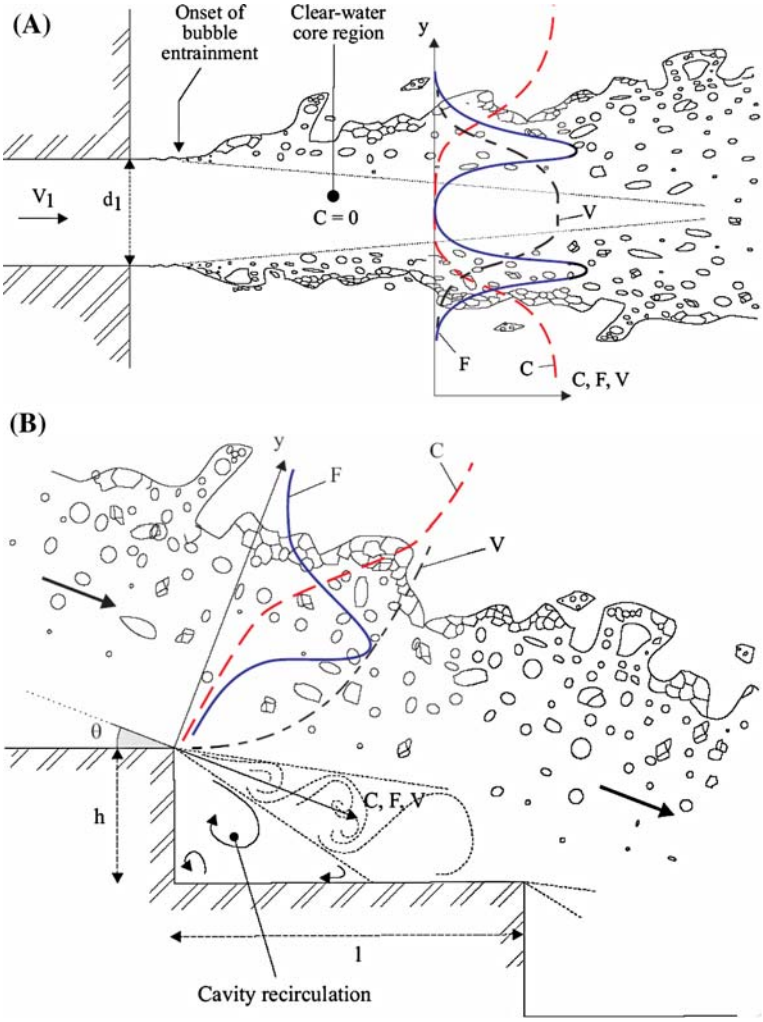

Fig. 6 Definition sketches of interfacial free-surface aeration (**a**) Interfacial aeration in a water jets discharging into atmosphere (**b**) Free-surface aeration in a skimming flow above a stepped invert

where U_w is the mean flow velocity ($U_w = q_w/d$), and C_{mean} is the depth-averaged void fraction defined as:

$$C_{mean} = \frac{1}{Y_{90}} \int_{y=0}^{y=Y_{90}} C \, dy \tag{13}$$

and C is the local void fraction varying with depth.

Despite some simplifications, Eq. 9, and even Eq. 12, highlights the large number of relevant dimensionless parameters in any study of interfacial free-surface aeration.

Table 2 Systematic studies of dynamic similarity and scale effects of air-water flow properties in skimming flows on stepped spillway chutes

Study (1)	Similitude (2)	Experimental flow conditions (3)	Instrumentation (4)	Experimental data (5)
[4]	Froude	$\theta = 30.0°$, h = 0.023, 0.046, 0.092 m $L_r = 1, 2, 4$ $\theta = 50.0°$, h = 0.031, 0.093 m $L_r = 1, 3$	Double-tip optical fibre probe	Void fraction & velocity distributions
[23]	Froude	$\theta = 3.4°$ h = 0.0715, 0.143 m $L_r = 1, 2$	Single-tip conductivity probe (Ø = 0.35 mm)	Void fraction & bubble count rate distributions
[35]	Froude	$\theta = 15.9°$ h = 0.05, 0.10 m $L_r = 1, 2$	Double-tip conductivity probe (Ø = 0.025 mm)	Void fraction, bubble count rate, velocity & turbulence distributions, Bubble sizes
[17]	Froude	$\theta = 21.8°$ h = 0.05, 0.10 m $L_r = 1, 2$	Single-tip conductivity probe (Ø = 0.35 mm) & Double-tip conductivity probe (Ø = 0.25 mm)	Void fraction, bubble count rate, velocity & turbulence distributions, Bubble sizes, Integral turbulent scales
	Reynolds	$\theta = 21.8°$ h = 0.05, 0.10 m $L_r = 1$	Single-tip conductivity probe (Ø = 0.35 mm) & Double-tip conductivity probe (Ø = 0.25 mm)	Void fraction, bubble count rate, velocity & turbulence distributions, Bubble sizes, Integral turbulent scales

Note: h, vertical step height; L_r, geometric scaling ratio; θ, chute slope

4.1 Physical modelling and scale effects in stepped spillways

Some systematic studies of the air–water flow properties in skimming flows on stepped spillway models were recently completed (Table 2). For a skimming flow above a stepped invert Eq. 9 may be extended:

$$C, \frac{Fd_c}{V_c}, \frac{V}{\sqrt{gd_c}}, \frac{u'}{V_c}, \frac{d_{ab}}{d_c} \ldots = F_5\left(\frac{x}{d_c}, \frac{y}{d_c}, \frac{z}{d_c}, \rho_w \frac{\sqrt{gd_c{}^3}}{\mu_w}, \frac{g\mu_w{}^4}{\rho_w \sigma^3}, \frac{h}{d_c}, \frac{W}{d_c}, \theta, \frac{k_s}{d_c}, \ldots\right) \tag{14}$$

where h is the vertical step height (Fig. 6b).

The validity of the Froude similitude were tested for a range of chute slopes $3.4° < \theta < 50°$, step heights $0.023 < h < 0.143$ m and with Reynolds numbers $\rho_w\sqrt{gd_c{}^3}/\mu_w$ up to 5 E+5 (Table 2). The results showed a lesser number of entrained bubbles and comparatively greater bubble sizes observed in the smallest models, as well as lower turbulence levels and larger turbulent length and time scales at the lowest Reynolds numbers based upon a Froude

similitude [17,35]. The findings had direct implications on stepped spillway design. Lesser turbulence levels in small laboratory flumes must imply a lesser rate of energy dissipation, particularly on long chutes. That is, small-size models are likely to underestimate the rate of energy dissipation of prototype stepped spillways for similar flow conditions. Similarly, the lesser number of entrained bubble sizes in laboratory flumes must affect the rate of air–water mass transfer on the chute. The experimental results implied that the air–water interface area, hence the rate of air–water mass transfer, are underestimated in small-size physical-models, and extrapolation are not reliable unless working at full scale (e.g., [50]). Chanson and Felder [17] tested also the validity of Reynolds similarity. The results showed that the Reynolds similitude was not suitable for the investigations of two-phase flow properties in skimming flows on a stepped spillway.

Importantly, all the results demonstrated that the selection of the flow property(ies) used to assess scale effects is essential. For example, BacaRa [2] and Chanson et al. [25] tested the flow resistance in skimming flow for a range of flow conditions. BacaRa [2] obtained results free of scale effects for $h \geq 0.028$ m, while Chanson et al. [25] concluded that a proper physical modelling of flow resistance required $h > 0.020$ m and $\rho_w \sqrt{g d_c^3} / \mu_w > 2.5$ E+4. But recent studies of local air–water flow properties (Table 2) showed that turbulence levels, entrained bubble sizes and interfacial areas were not properly scaled by a Froude similitude with Reynolds numbers up to 5 E+5 [17,18].

Despite the specific features of the stepped invert, it is believed that the results are applicable to a wide range of interfacial aeration processes.

5 Discussion

The effects of surfactant and biochemical properties and water salinity are relevant to the studies of air entrainment in breaking waves and industrial processes involving sea- and salt-waters. Comparative studies of bubble entrainment in freshwater and seawater are scarce (e.g., [42,48]). Some studies considered the size of bubbles produced by a frit, showing that bubble coalescence was drastically reduced in saltwater compared to freshwater experiments at a 1:1 scale ($L_r = 1$).

An experimental study in the developing flow region of vertical plunging jets was conducted and identical experiments were repeated ($L_r = 1$) with freshwater, natural seawater and artificial saltwater [24,27]. The data showed lesser air entrainment in saline waters. The results indicated further lesser air entrainment in natural seawater than in artificial saltwater, all inflow parameters being identical ($L_r = 1$). It was hypothesised that surfactants, biological and chemical elements harden the induction trumpet (Fig. 4a) and diminish air entrapment at impingement in seawater. The results implied that classical dimensional analysis is incomplete unless physical, chemical and biological properties other than density, viscosity and surface tension are taken into account.

Furthermore, Eqs. 7 and 9 did not account for the characteristics of the instrumentation. The type of instrumentation, the size of the probe sensor, the sampling rate and possibly other probe characteristics do affect the minimum bubble size detectable by the instrumentation. In the particular case of phase-detection intrusive probes, bubble chords smaller than the probe sensor cannot be detected while bubble chord times smaller than the scan period (i.e., inverse of sampling rate) are not recorded.

To date most systematic studies of scale effects affecting air entrainment processes were conducted mostly with the same instrumentation and sensor size in all experiments (Tables 1 and 2). That is, the probe sensor size was not scaled down in the small size models. It must

be acknowledged that this aspect might become a constraint and limitation. It is believed that the only systematic investigation on the effects of the probe sensor size is a series of two studies of air entrainment in skimming flows in stepped spillways [9,22]. In each case, the air–water flow measurements were repeated with identical flow conditions and chute geometry and instrumentation technique, but different sensor sizes. The performances of phase-detection conductivity probes were tested for two sensors sizes: 25 µm (0.025 mm) and 350 µm (0.35 mm) with the same sampling rates. The results indicated consistently larger bubble count rate measurements with the smaller 0.025 mm sensor probe and a broader range of bubble/droplet sizes detected by the 0.025 mm sensor probe than by the 0.35 mm sensor probe. For example, with a dimensionless step height $h/d_c = 0.85$ and $\rho_w\sqrt{g d_c^3}/\mu_w = 1.26\,E{+}5$, the bubble chord sizes measured with the 0.35 mm sensor were typically 18 to 50% larger (28% in average) than the chord lengths measured with the 0.025 mm sensor [9].

6 Summary and conclusion

In hydraulic structures, the turbulent flows are characterised by significant air entrainment associated with strong interactions between entrained bubbles and turbulent structures. The current expertise in air–water flows relies upon laboratory experiments performed under controlled flow conditions. The physical studies are typically designed using a Froude similitude which implies drastically smaller Reynolds numbers than in the corresponding prototype flows. There are therefore some critical issues with the validity of model result extrapolation to prototype flow conditions.

The two fundamental mechanisms of air entrainment were reviewed: i.e, singular entrapment and interfacial aeration. Typical examples of singular aeration included the hydraulic jump and the plunging jet, while interfacial aeration applications encompassed self-aerated open channel flows and water jets discharging into atmosphere (Fig. 2). Basic dimensional analyses were developed for both singular and interfacial aeration processes. The results were discussed in the light of very recent systematic investigations (Tables 1 and 2). They demonstrated that the notion of scale effects is closely linked with the selection of some characteristic air–water flow property(ies): e.g., void fraction distributions, turbulence levels, or air–water interface area. Recent studies of local air–water flow properties highlighted that turbulence levels, entrained bubble sizes and interfacial areas were not properly scaled according to a Froude similitude even in large-size models operating with $\rho_w\, q_w/\mu_w$ up to 5 E+5. In laboratory models, the dimensionless turbulence levels, air–water interfacial areas and mass transfer rates were drastically underestimated.

An alternative approach may be based upon self-similarity considerations. Self-similarity is closely linked with dynamic similarity [3]. While Eqs. 7 and 9 showed that it is impossible to achieve a true dynamic similarity in small-size models, some experimental results showed a number of self-similar relationships that remained invariant under changes of scale (e.g. [16]). These relationships had scaling symmetry which led in turn to remarkable application at prototype scales. These findings were significant because they may provide a picture general enough to be used, as a first approximation, to characterise the air–water flow field in similar prototype structures.

Despite some active research, the turbulent air–water flows remain some fascinating 'white water' phenomenon that is still poorly understood. Numerical modelling may be a future research direction. The numerical approach will not be easy because the air–water flows encompass many challenges including two-phase flow structures, turbulence and free surface. Presently, some numerical techniques (LES, VOF) can be applied to turbulent flows with

large Reynolds numbers, but they lack microscopic resolutions and the results are not always reliable. Other numerical techniques (DNS) provide a greater level of small-scale details but are limited to turbulent flows with relatively small Reynolds numbers. Future studies may be based upon some 'composite' models embedding numerical and physical studies.

Acknowledgements The writer thanks Graham ILLIDGE and Clive BOOTH (The University of Queensland) for their technical assistance. He further acknowledge the many students and co-workers involved in the project, including Giovanna CAROSI (Italy), Stefan FELDER (Germany), Dr Carlos GONZALEZ (Australia), and Dr Frédéric MURZYN (France).

References

1. Anwar HO (1994) Self-aerated flows on chutes and spillways—discussion. J Hydraul Eng ASCE 120(6):778–779
2. BaCaRa (1991) Etude de la Dissipation d'Energie sur les Evacuateurs à Marches. (Study of the energy dissipation on stepped spillways) *Rapport d'Essais*, Projet National BaCaRa, CEMAGREF-SCP, Aix-en-Provence, France, October, 111 pp (in French)
3. Barenblatt GI (1996) Scaling, self-similarity, and intermediate asymptotics. Cambridge University Press, UK, 386 pp
4. Boes RM (2000) Scale effects in modelling two-phase stepped spillway flow. In: Minor HE, Hager WH (eds) International workshop on hydraulics of stepped spillways. Balkema Publ, Zürich, pp 53–60
5. Boes RM, Hager WH (2003) Two-phase flow characteristics of stepped spillways. J Hydraul Eng ASCE 129(9):661–670; discussion 131(5):419–429
6. Brocchini M, Peregrine DH (2001) The dynamics of strong turbulence at free surfaces. Part 2. Free-surface boundary conditions. J Fluid Mech 449:255–290
7. Cain P (1978) Measurements within self-aerated flow on a large spillway. PhD Thesis, Ref. 78–18. Department of Civil Engineering, University of Canterbury, Christchurch, New Zealand
8. Cain P, Wood IR (1981) Instrumentation for aerated flow on spillways. J Hydraul Div ASCE 107(HY11):1407–1424
9. Carosi G, Chanson H (2006) Air–water time and length scales in skimming flows on a stepped spillway. Application to the spray characterisation. Report No. CH59/06. Division of Civil Engineering, The University of Queensland, Brisbane, Australia, July, 142 pp
10. Cartellier A, Achard JL (1991) Local phase detection probes in fluid/fluid two-phase flows. Rev Sci Instrum 62(2):279–303
11. Chanson H (1993) Self-aerated flows on chutes and spillways. J Hydraul Eng ASCE 119(2):220–243; discussion 120(6):778–782
12. Chanson H (1995) Air bubble diffusion in supercritical open channel flow. In: Bilger RW (ed) Proceedings of 12th Australasian fluid mechanics conference AFMC, vol 2, Sydney, Australia, pp 707–710
13. Chanson H (1997) Air bubble entrainment in free-surface turbulent shear flows. Academic Press, London, 401 pp
14. Chanson H (2002) Air–water flow measurements with intrusive phase-detection probes. Can we improve their interpretation? J Hydraul Eng ASCE 128(3):252–255
15. Chanson H (2004) The hydraulics of open channel flow: an introduction, 2nd edn. Butterworth-Heinemann, London, 630 pp
16. Chanson H, Carosi G (2007) Turbulent time and length scale measurements in high-velocity open channel flows. Exp Fluids 42(3):385–401. doi:10.1007/s00348-006-0246-2
17. Chanson H, Felder S (2007) Dynamic similarity and scale effects in turbulent free-surface flows above triangular cavities. In: Jacobs P, Mcintyre T, Cleary M, Buttsworth D, Mee D, Clements R, Morgan R, Lemckert C (eds) Proceedings of 16th Australasian Fluid Mechanics Conference AFMC, Gold Coast, Australia, 2–7 December, pp 691–698 (CD-ROM)
18. Chanson H, Gonzalez CA (2005) Physical modelling and scale effects of air–water flows on stepped spillways. J Zhejiang Univ Sci 6A(3):243–250
19. Chanson H, Gualtieri C (2008) Similitude and scale effects of air entrainment in hydraulic jumps. J Hydraul Res IAHR 46(1):35–44
20. Chanson H, Manasseh R (2003) Air entrainment processes in a circular plunging jet. Void fraction and acoustic measurements. J Fluids Eng Trans ASME 125(5):910–921
21. Chanson H, Toombes L (2002a) Air–water flows down stepped chutes: turbulence and flow structure observations. Int J Multiphase Flow 28(11):1737–1761

22. Chanson H, Toombes L (2002b) Experimental study of gas–liquid interfacial properties in a stepped cascade flow. Environ Fluid Mech 2(3):241–263
23. Chanson H, Toombes L (2002c) Energy dissipation and air entrainment in a stepped storm waterway: an experimental study. J Irrig Drain Eng ASCE 128(5):305–315
24. Chanson H, Aoki S, Hoque A (2002a) Similitude of air bubble entrainment and dispersion in vertical circular plunging jet flows. An experimental study with freshwater, salty freshwater and seawater. Coastal/Ocean Engineering Report No. COE02-1. Department of Architecture and Civil Engineering, Toyohashi University of Technology, Japan, 94 pp
25. Chanson H, Yasuda Y, Ohtsu I (2002b) Flow resistance in skimming flows and its modelling. Can J Civil Eng 29(6):809–819
26. Chanson H, Aoki S, Hoque A (2004) Physical modelling and similitude of air bubble entrainment at vertical circular plunging jets. Chem Eng Sci 59(4):747–754
27. Chanson H, Aoki S, Hoque A (2006) Bubble entrainment and dispersion in plunging jet flows: freshwater versus seawater. J Coastal Res 22(3):664–677
28. Chirichella R, Gomez Ledesma R, Kiger KT, Duncan JH (2002) Incipient air entrainment in a translating axisymmetric plunging laminar jet. Phys Fluids 14(2):781–790; discussion 14(9):3367–3368
29. Crowe C, Sommerfield M, Tsuji Y (1998) Multiphase flows with droplets and particles. CRC Press, Boca Raton, 471 pp
30. Cummings PD, Chanson H (1999) An experimental study of individual air bubble entrainment at a planar plunging jet. Chem Eng Res Design Trans I-Chem E, Part A 77(A2):159–164
31. Ehrenberger R (1926) Wasserbewegung in steilen Rinnen (Susstennen) mit besonderer Berucksichtigung der Selbstbelüftung. (Flow of water in steep chutes with special reference to self-aeration) Zeitschrift des Österreichischer Ingenieur und Architektverein, No. 15/16 and 17/18 (in German) (Trans: Wilsey EF, U.S. Bureau of Reclamation)
32. El Hammoumi M (1994) Entraînement d'Air par Jet Plongeant Vertical. Application aux Becs de Remplissage pour le Dosage Pondéral (Air entrainment by vertical plunging jet. application to refill nozzles applied to dosage). PhD thesis, INPG, Grenoble, France (in French)
33. Ervine DA, Falvey HT (1987) Behaviour of turbulent water jets in the atmosphere and in plunge pools. Proc Instn Civ Engrs. London, Part 2, March 1987, 83:295–314; discussion: Part 2, March–June 1988, 85:359–363
34. Ervine DA, Mckeogh EJ, Elsawy EM (1980) Effect of turbulence intensity on the rate of air entrainment by plunging water jets. Proc Instn Civ Engrs, Part 2, June, pp 425–445
35. Gonzalez CA, Chanson H (2004) Interactions between cavity flow and main stream skimming flows: an experimental study. Can J Civ Eng 31(1):33–44
36. Henderson FM (1966) Open channel flow. MacMillan Company, New York
37. Heraud D (1966) Dispersion des Jets Liquides; Influence des Rugosités de Paroi. PhD thesis, University Grenoble 1, France
38. Hinze JO (1955) Fundamentals of the hydrodynamic mechanism of splitting in dispersion processes. J AIChE 1(3):289–295
39. Hoyt JW, Taylor JJ (1977) Waves on water jets. J Fluid Mech 83(Pt 1):119–127
40. Keller RJ (1972) Field measurement of self-aerated high speed open channel flow. PhD thesis, Department of Civil Engineering, University of Canterbury, New Zealand
41. Kobus H (1984) Scale effects in modelling hydraulic structures. Proceedings of international symposium on scale effects in modelling hydraulic structures. IAHR, Esslingen, Germany
42. Kolaini AR (1998) Sound radiation by various types of laboratory breaking waves in fresh ans salt water. J Acoust Soc Am 103(1):300–308
43. Mckeogh EJ (1978) A study of air entrainment using plunging water jets. PhD thesis, Queen's University of Belfast, UK, 374 pp
44. Murzyn F, Chanson H (2007) Free surface, bubbly flow and turbulence measurements in hydraulic jumps. Report CH63/07, Division of Civil Engineering, The University of Queensland, Brisbane, Australia, August, 116 pp, ISBN 9781864998917
45. Rajaratnam N (1962) An experimental study of air entrainment characteristics of the hydraulic jump. J Inst Eng India 42(7):247–273
46. Rao NSL, Kobus HE (1971) Characteristics of self-aerated free-surface flows. Water and waste water/current research and practice, vol 10. Eric Schmidt Verlag, Berlin, Germany
47. Resch FJ, Leutheusser HJ (1972) Le Ressaut Hydraulique: mesure de Turbulence dans la Région Diphasique. J La Houille Blanche 4:279–293
48. Scott JC (1975) The preparation of water for surface clean fluid mechanics. J Fluid Mech 69(Part 2):339–351

49. Straub LG, Anderson AG (1958) Experiments on self-aerated flow in open channels. J Hydraul Div Proc ASCE 84(HY7):1890-1–1890-35, paper 1890
50. Toombes L, Chanson H (2005) Air–water mass transfer on a stepped waterway. J Environ Eng ASCE 131(10):1377–1386
51. Wood IR (1991) Air entrainment in free-surface flows. IAHR hydraulic structures design manual no. 4, Hydraulic design considerations. Balkema Publ., Rotterdam, The Netherlands, 149 pp